Multi Cantilever-Mass Mechanism for Vibration Suppression

Péter Szuchy[1], Lívia Cveticanin[2], István Bíró[3]

[1,2]Doctoral School on Safety and Security Sciences, Óbuda University, Népszínház u. 8, 1081 Budapest, Hungary, cpinter.livia@bgk.uni-obuda.hu

[1,3]Department of Mechanics, Faculty of Engineering, University of Szeged, Mars tér 7, 6724 Szeged, Hungary, gi@mk.u-szeged.hu

Abstract: In this paper a new type of passive mechanism for vibration suppression is introduced. The mechanism is based on the system of cantilever – mass units (dynamic absorbers) connected to the basic structure. The support of cantilevers is rigid or even elastic. The vibration of the system is caused by external excitation force which acts on the basic structure. The aim of the paper is to determine the parameters of the system for which the frequency gap and the vibration suppression occur. The used mathematical model is a system of coupled equations where the measured parameters are introduced by the application of a newly developed, so-called, 'elastic support method'. Solving the mathematical model, the amplitude-frequency vibration property of the system is obtained. The computed solution is compared with that the previously published result of the 'wallpaper' type metastructure for vibration suppression, which is modeled as a system of translation moving system of mass-in-mass units. It is concluded that the effect of the suggested mechanism is in good agreement with that of the metastructure for vibration suppression. The resonances of the two models are matched with the results of Inventor Finite Element Analysis, too. Difference in results is negligible.

Keywords: "wallpaper"-like metamaterial; cantilever-mass mechanism; vibration suppression; 5-DoF system; natural-frequency

1 Introduction

Recently, mechanical metastructures and metamaterials are developed for suppression or elimination of vibration. Metamaterials and metastructures are artificially composed systems containing a basic mass in which small masses are added [1-4]. The added masses have the role of vibration absorbers. Opposed to the conventional materials, the metastructure absorbers are integrated into the basic material [5]. Metastructures are modeled as complex systems of mass-in-mass units where properties of the added mass-spring unit satisfy the condition for dynamic absorber of the basic mass [6-9]. Various types of metastructures are already

developed: in-line 1D or bar structures [10-13], space structures [14-15] and plane or wall panels [16-18]. The main disadvantage of all of these metastructures is the complexity of their fabrication. The new types of metastructures have absorbers made of the same material as the basic structure and the system is constructed as a single unit. The 3D printing technique allows creation of such structures, with extremely complex geometries tuned for broadband vibration suppression, for example a square structure inside of which mass as absorbers act [19-21] or stick – like resonator [22]. Such 3D-printed metastructures are suitable for passive vibration suppression. In addition, the structures remain capable of bearing loads without adding additional mass. For all of the mentioned metamaterials, it is common that they suppress vibration in certain frequency region [23, 24], and the width of the band gap, where the decrease of the amplitude of vibration occurs, is very small.

To eliminate these lacks, the system with the higher number of dynamic absorbers [25] and nonlinear properties [26] are introduced. Thus, the 'wallpaper'-like metastructure which contains 5 different dynamic absorbers is able to admit 5 different vibration frequencies [18]. In spite of the fact that the design seems to be simple (between a basic plane and an external surface with cups masses are settled (see Fig. 1) which move translator up and down due to the action of the vertical external excitation), fabrication with proper values for vibration suppression is not an easy task.

In this paper the new multicantilever-mass mechanism for vibration suppression is developed.

The aim of the new mechanism is to eliminate vibration on certain frequencies, of all the unwilling ones. The requirements for vibration elimination directly influence the design of the mechanism and the number of cantilever-mass dynamic absorbers. In the paper, dynamics of the mechanism is mathematically modeled. Parameters of the model are included by using the new, so-called 'elastic support method', springing from measured values. After solving the equation of the oscillatory motion, the results are applied for parameter analysis of the mechanism. The new mechanism with 5 cantilever-masses is compared with the 5-DoF wallpaper like metastructure. It is observed that the comparison is possible and that the parameters of the new model are more controllable than the previously developed wallpaper like metastructure with the translation motion of masses. The resonance cases of both models are matched using of Inventor Finite Element Analysis. Difference in results is negligible.

The paper has 5 sections. After the introduction in Section 2, the physical and mathematical model of the cantilever-mass mechanism is developed. The system is described with n linear coupled second order differential equations. In Section 3, a new method for calculation of the stiffness of the elastic support is developed. In Section 4, the amplitude-frequency vibration property of the 5-DoF cantilever-mass mechanism is obtained. The result is compared with that obtained for the 5-DoF

'wallpaper' type mechanism with translator motion. The solution is matched with the results of Inventor Finite Element Analysis (FEA) of the 3D solid body. The paper ends with conclusions.

2 Model of the Mechanism

In this section, the physical and mathematical model of the cantilever-mass mechanism is developed.

2.1. Physical Model of the Cantilever-Mass Mechanism

Based on the principle of the 'wallpaper' metastructure, but keeping the practical needs of measuring in mind, the translational model (Fig. 1) is changed into the cantilever beam model (Fig. 2). The cantilever-mass mechanism for vibration suppression is physically modelled as a system of beams clamped at one end with concentrated masses on the other end, which are attached to the primary structure. The primary structure is modelled as a clamped beam-mass unit (Fig. 2a), where the rigidity of the beam is EI_1 and the mass is m_1. On the mass m_1, the periodic excitation force $F(t)$ acts, which causes vibrations. Each added unit, which represents a dynamic absorber, contains a cantilever of transversal rigidity EI_i, a length b_i, and concentrated mass m_i. Only one damper with coefficient k_1 remained. The number of units is not limited, it depends on the requirement for elimination of vibrations of the basic element 1.

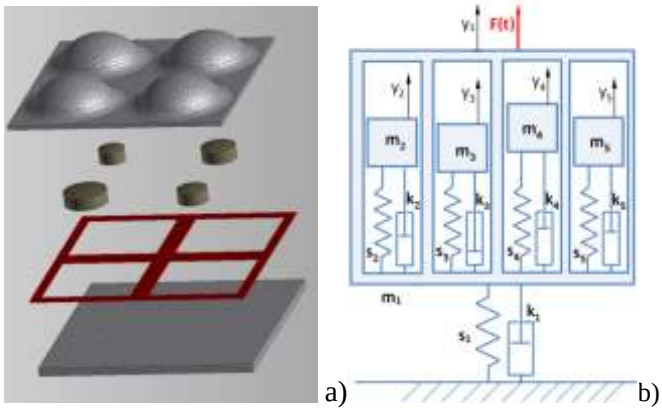

Figure 1

"Wall-paper"-like metastructure: a) Exploded view of the 3D model; b) 5-DoF translational model

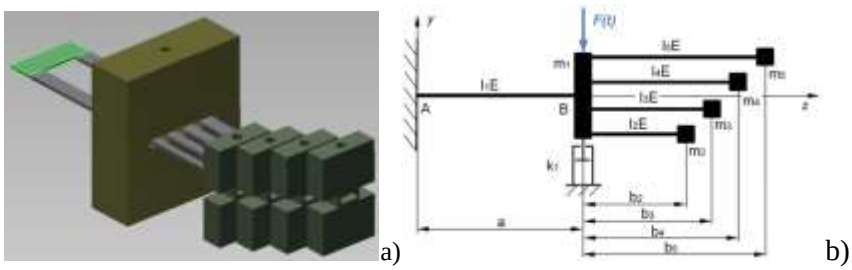

Figure 2
The 5-DoF cantilever-mass mechanism: a) 3D solid body model; b) Scheme of model

2.2. Mathematical Model of the Cantilever-Mass Mechanism

Let us consider the mathematical model of the multicantilever-mass mechanism where on the basic structure 1, the i=2,3,…n absorber units are attached (see Fig. 2b). It is supposed that the beam bending is in one plane. In addition, the movement of discrete masses is assumed to be in-line.

The bending position of each mass m_j is obtained by applying the Betti theorem summarizing the deflection of the mass m_1 caused by the external force, deflections of m_j due to external and inertial force and the displacement caused by interaction between added masses of the absorber.

Using the linear bending theory, the displacement of the mass m_1 under influence of the force F_1 is obtained as

$$y_B = \frac{F_1 a^3}{3\, I_1 E} \tag{1}$$

where a is the position of the mass, i.e. the length of the beam 1. It gives the inverse rigidity coefficient

$$c_{11} = \frac{y_B}{F_1} = \frac{a^3}{3\, I_1 E} \tag{2}$$

However, the force F_1 causes bending of all beams in the system and the bending position of masses m_i are

$$y_{Ci} = \frac{F_1 a^2 (2a+3b_i)}{6\, I_1 E} \tag{3}$$

The corresponding inverse rigidity coefficients are

$$c_{1i} = \frac{a^2 (2a+3b_i)}{6\, I_1 E} \tag{4}$$

where i=2,3,...n.

According to the force F_i, which directly acts on m_i, the displacements are

$$y_{Ci} = \frac{F_i a(a^2+3ab_i+3b_i^2)}{3\, I_1 E} + \frac{F_i b_i^3}{3\, I_i E} \tag{5}$$

and the inverse rigidity coefficients follow as

$$c_{ii} = \frac{a(a^2+3ab_i+3b_i^2)}{3\, I_1 E} + \frac{b_i^3}{3\, I_i E} \tag{6}$$

The force F_i which acts on m_i has also an influence on the other masses m_j of the mechanism. Thus, for i,j=2,3,...n, $i \neq j$ the displacement is

$$y_{Ci} = \frac{F_2 a^3}{3\, I_1 E} + \frac{b_2 F_2 a^2}{2\, I_1 E} + \left(\frac{F_2 a^2}{2\, I_1 E} + \frac{b_2 F_2 a}{I_1 E}\right) b_3 = \frac{F_i a(2a^2+3ab_i+3ab_j+6b_i b_j)}{6\, I_1 E} \tag{7}$$

and the corresponding inverse rigidity coefficient

$$c_{ij} = \frac{a(2a^2+3ab_i+3ab_j+6b_i b_j)}{6\, I_1 E} \tag{8}$$

Remark: There is the symmetry of the rigidity coefficients, and for $i \neq j$ it yields $c_{ij}=c_{ji}$, where i,j=2,3,...n.

Using the previous consideration, the total deflection of each mass (including the mass m_1) is calculated as

$$y_i + \sum_{j=1}^{n} c_{ij} F_j = 0 \qquad i = 2,3 \dots n \tag{9}$$

Introducing the inertial, damping and excitation force acting on mass m_1,

$$F_1 = m_1 \ddot{y}_1 + k_1 \dot{y}_1 - F_0 \sin \omega_g t \tag{10}$$

and forces acting on masses m_j, where j=2,3,...n

$$F_j = m_j \ddot{y}_j + k_j \dot{y}_j \tag{11}$$

the system of differential equations of motion for the system follows as

$$\boldsymbol{M}\ddot{\boldsymbol{y}} + \boldsymbol{K}\dot{\boldsymbol{y}} + \boldsymbol{C^{-1}}\boldsymbol{y} = \boldsymbol{F} \tag{12}$$

where **C** is the symmetric matrix of the inverse rigidity coefficients, ***K*** is the damping matrix, ***M*** is the mass matrix, i.e.

$$\boldsymbol{C} = \begin{bmatrix} c_{11} & c_{12} & \dots & c_{1n} \\ c_{21} & c_{22} & \dots & c_{2n} \\ \dots & \dots & \dots & \dots \\ c_{n1} & c_{n2} & \dots & c_{nn} \end{bmatrix}, \qquad \boldsymbol{K} = \begin{bmatrix} k_1 & 0 & \dots & 0 \\ 0 & k_2 & \dots & 0 \\ \dots & \dots & \dots & \dots \\ 0 & 0 & \dots & k_n \end{bmatrix}, \qquad \boldsymbol{M} = \begin{bmatrix} m_1 & 0 & \dots & 0 \\ 0 & m_2 & \dots & 0 \\ \dots & \dots & \dots & \dots \\ 0 & 0 & \dots & m_n \end{bmatrix}$$

$$\boldsymbol{y} = [y_1, y_2, \dots., y_n] \quad \text{and} \quad \boldsymbol{F} = \left[F_0 sin\omega_g t, 0, \dots., 0\right]. \tag{13}$$

The equation (12) is a system of *n* coupled second order differential equations which describes the absorber motion. Solving the system (12), the amplitude-frequency relations are obtained.

3 Model of the Beam Fixed in an Elastic Support

The model (12) corresponds to the case when masses of cantilevers are omitted. If the mass of the cantilever is as significant as the value of added mass, it has to be taken into consideration. It is supposed that the mass of the beam is continually distributed along its length, the total mass of the basic beam is m_{r1}, while the masses of the beams in mechanism are m_{ri}, where i=2,3,…n. Reducing masses of beams in the position B of the basic mass (Fig. 3a) the total masses m_{red1} and m_{redi} (i=2,3,…n) are obtained.

Thus, for the system which contains only one added cantilever beside the basic one (Fig. 3a), the reduced mass in B is obtained by equating the kinetic energy of the distributed and point masses, i.e.

$$\frac{1}{2}m_{red1}\dot{y}_B^2 = \frac{1}{2}\frac{m_{r1}}{a}\int_0^a (\dot{y}_1(z))^2\,dz, \qquad \frac{1}{2}m_{red2}\dot{y}_B^2 = \frac{1}{2}\frac{m_{r2}}{b_2}\int_a^{a+b_2} (\dot{y}_2(z))^2\,dz \tag{14}$$

where $\dot{y}_B$ is the velocity of B, $\dot{y}_1(z)$ and $\dot{y}_2(z)$ is velocity distribution along the beam 1 and 2, respectively.

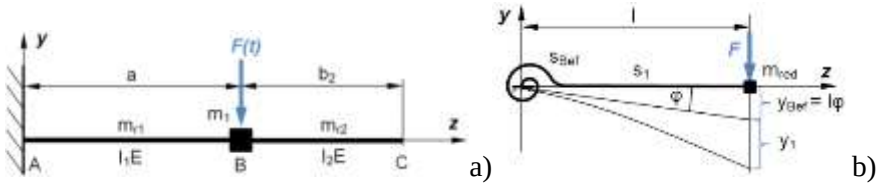

Figure 3
Scheme of the cantilever supported: a) rigid; b) elastic

Using the assumption that there is a direct correlation between the velocity $\dot{y}$ and displacement y i.e. $\frac{\dot{y}(z)}{\dot{y}_B} = \frac{y(z)}{y_B}$ where $\dot{y}_B$ is the velocity and y_B is the displacement of B, equations (14) transform into

$$\frac{1}{2}m_{red1}\dot{y}_B^2 = \frac{1}{2}\frac{m_{r1}}{a}\frac{\dot{y}_B^2}{y_B^2}\int_0^a (y_1(z))^2\,dz, \qquad \frac{1}{2}m_{red2}\dot{y}_B^2 = \frac{1}{2}\frac{m_{r2}}{b_2}\frac{\dot{y}_B^2}{y_B^2}\int_a^{a+b_2} (\dot{y}_2(z))^2\,dz \tag{15}$$

where the deflection of B is $y_B = \frac{Fa^3}{3I_1E}$ and the elastic lines of AB and BC [14]

$$y_1(z) = \frac{F}{6I_1E}(3az^2 - z^3), \;\; y_2(z) = \frac{Fa^2}{6I_1E}(3z - a). \tag{16}$$

After integration of (15) with (16) and some modifications, the reduced masses $m_{red1}$and m_{red2} are obtained as

$$m_{red1} = \frac{33}{140}m_{r1}, \qquad m_{red2} = m_{r2}\frac{3(a+b_2)^2+a^2}{4a^2} \tag{17}$$

Usually, it is assumed that the cantilever is connected with the rigid support. However, in multicantilever-mass mechanism, the units are elastically supported. In the next section, a method is developed for including the effect of elastic support in the rigidity coefficient of the system. The method represents a mixed analytic-experimental one, where the measured vibration values are incorporated into the model of the system.

3.1. Correction of Stiffness Matrix using the 'Elastic Supporting Method'

The procedure for including correction in the coefficient of rigidity of the system due to elastic support is named 'elastic supporting method'. On the system with reduced mass m_{red} and a beam, with length l and rigidity s_1, clamped in elastic support with rigidity s_{Bef}, the excitation force F acts (Fig. 3b). It causes the displacement of B, which is the sum of the bending of the beam y_1 and displacement y_{Bef} due to inclination for angle φ. For the inverse rigidity of the beam $c_1 = \frac{Fl^2}{3IE}$, the bending displacement is

$$y_1 = Fc_1 \tag{18}$$

It is assumed that the displacement of B due to the bending torque Fl is the linear function of the inclination angle φ. For $\varphi = (Fl)c_{Bef}$ and $y_{Bef} = l\varphi$, the displacement is

$$y_{Bef} = Fc_{Bef}l^2 \tag{19}$$

where c_{Bef} is the inverse rigidity coefficient of support and l is the length of the beam. Finally, due to elasticity of the beam and of the elastic connection, the total displacement in B is

$$y = y_{Bef} + y_1 = l\varphi + \frac{Fl^3}{3IE} = F(c_{Bef}l^2 + c_1) \tag{20}$$

According to (20) the reduced inverse rigidity coefficient follows as

$$c_{red} = \frac{y}{F} = c_{Bef}l^2 + c_1 \tag{21}$$

For the reduced inverse rigidity (21) and reduced mass (17), the frequency of vibration is obtained in the form

$$f_m = \frac{1}{2\pi}\sqrt{\frac{1}{c_{red}m_{red}}} = \frac{1}{2\pi}\sqrt{\frac{1}{(c_{Bef}l^2+l^3/3IE)m_{red}}} \tag{22}$$

where $m_{red} = m_1 + m_{red1} + m_{red2}$

Relation (22) is suitable for determination of the unknown rigidity coefficient c_{Bef}. Measuring the frequency of vibration of the model and substituting the obtained value into (22), the rigidity coefficient of the support c_{Bef} is calculated. The method for obtaining of the unknown rigidity suggested in the paper is a mixed procedure which interacts the data of the measurement and the analytically computed value.

To prove the accuracy of the suggested method, the comparison of calculated rigidity coefficient of a 1-DoF flexible cantilever-mass beam with experimentally obtained one is done (see Fig. 4). Position of the mass in the mechanism is varied and the frequency of the system is changed. In spite of that, it is obtained that both the calculated and the measured inverse rigidity coefficient of support c_{Bef} remain almost constant. Difference between measured and computed values is negligible.

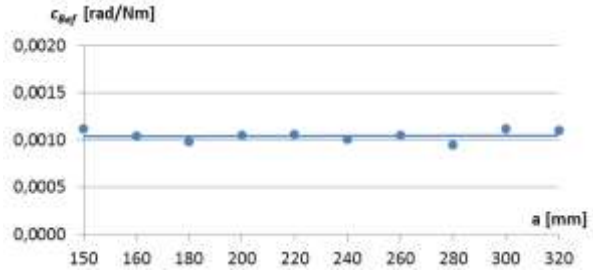

Figure 4

Inverse rigidity coefficient of support (c_{Bef}) of 1-DoF flexible clamped cantilever beam for different positions of mass m_1 (a) obtained by measuring (dots) and by computed trend curve (full line)

Using the suggested procedure, the elements of the symmetric matrix **C,** where the inverse rigidity coefficient of support is included, are calculated as

$$c_{11} = c_b a^2 + \frac{a^3}{3\,I_1 E} \tag{23}$$

$$c_{1i} = c_{i1} = c_b(a^2 + ab_i) + \frac{a^2(2a+3b_i)}{6\,I_1 E}, \quad (i = 2 \dots 5) \tag{24}$$

$$c_{ii} = c_b(a + b_i)^2 + \frac{a(a^2+3ab_i+3b_i^2)}{3\,I_1 E} + \frac{b_i^3}{3\,I_i E}, \quad (i = 2 \dots 5) \tag{25}$$

$$c_{ij} = c_{ji} = c_b\left[a^2 + a\left(b_i + b_j\right) + b_i b_j\right] + \frac{a\left[2a^2+3a(b_i+b_j)+6b_i b_j\right]}{6\,I_1 E}, \quad (i,j = 2 \dots 5, i \neq j)\mathrm{c_{ij}} = \mathrm{c_{ji}} = \mathrm{c_b}\left[\mathrm{a^2 + a\left(b_i + b_j\right) + b_i b_j}\right] + \frac{\mathrm{a\left[2a^2+3a(b_i+b_j)+6b_i b_j\right]}}{\mathrm{6\,I_1 E}}, \quad (\mathrm{i,j} = 2 \dots 5, \mathrm{i} \neq \mathrm{j}) \tag{26}$$

It is important to emphasize that the effect of the inverse rigidity coefficient of support on the frequency of the system is up to 20%.

During experimental investigation it is seen that the value of the inverse rigidity coefficient of support is influenced by several factors (including the structure of the vise, the supporting force and the material of the support soil).

4 Comparison of Vibration Properties of the Translational and the Cantilever-Mass Models

In our investigation, the 5-DoF cantilever-mass mechanism which contains 4 absorbers settled on the basic mass m_1 is considered (Fig. 2b). Motion of the beams is assumed to be only in one plane and of the end points in vertical direction. Using the AutoCAD Inventor Software the 3D solid body system is created (Fig. 2a). Parameters of the mechanism are: a=0.12 m, b_2=0.11 m, b_3=0.13 m, b_4=0.15 m, b_5=0.17 m, m_1=4.000 kg, m_2=m_3=m_4=m_5=0.500 kg, ρ=7850 kg/m^3; E=210 GPa, I_1E=12.285 Nm^2, I_2E=2.835 Nm^2, I_3E=3.78 Nm^2, I_4E=4.725 Nm^2, I_5E=5.67 Nm^2. As masses of the springs are less than 10% of the attached masses, they are omitted in calculation. In addition, the elastic supporting and damping of the system are also neglected (in translational model k_i=0,0001 Ns/m, avoiding divide by zero). Based on the 3D solid body model and using the relations (23)-(26), the stiffness coefficients $(s_i, i = 1 \dots 5)$ of the cantilever beams are computed for the translational modell

$$s_1 = 1/c_{11} \tag{27}$$

$$s_i = \frac{3I_iE}{b_i^3}, \quad (i = 2 \dots 5) \tag{28}$$

Using the Cramer's rule for inverse stiffness matrix and the relations (27) and (28), the amplitude of vibration A_{1m} of the cantilever beam with mass m_1 excited with frequency ω_g is obtained

$$A_{1m} = \frac{\begin{vmatrix} F_0 & 0 & 0 & 0 & 0 \\ 0 & C_{22}^{-1}-m_2\omega_g^2 & C_{23}^{-1} & C_{24}^{-1} & C_{25}^{-1} \\ 0 & C_{32}^{-1} & C_{33}^{-1}-m_3\omega_g^2 & C_{34}^{-1} & C_{35}^{-1} \\ 0 & C_{42}^{-1} & C_{43}^{-1} & C_{44}^{-1}-m_4\omega_g^2 & C_{45}^{-1} \\ 0 & C_{52}^{-1} & C_{53}^{-1} & C_{54}^{-1} & C_{55}^{-1}-m_5\omega_g^2 \end{vmatrix}}{\begin{vmatrix} C_{11}^{-1}-m_1\omega_g^2 & C_{12}^{-1} & C_{13}^{-1} & C_{14}^{-1} & C_{15}^{-1} \\ C_{21}^{-1} & C_{22}^{-1}-m_2\omega_g^2 & C_{23}^{-1} & C_{24}^{-1} & C_{25}^{-1} \\ C_{31}^{-1} & C_{32}^{-1} & C_{33}^{-1}-m_3\omega_g^2 & C_{34}^{-1} & C_{35}^{-1} \\ C_{41}^{-1} & C_{42}^{-1} & C_{43}^{-1} & C_{44}^{-1}-m_4\omega_g^2 & C_{45}^{-1} \\ C_{51}^{-1} & C_{52}^{-1} & C_{53}^{-1} & C_{54}^{-1} & C_{55}^{-1}-m_5\omega_g^2 \end{vmatrix}} \tag{29}$$

In Fig. 5 the amplitude diagram as the function of the excitation frequency is plotted.

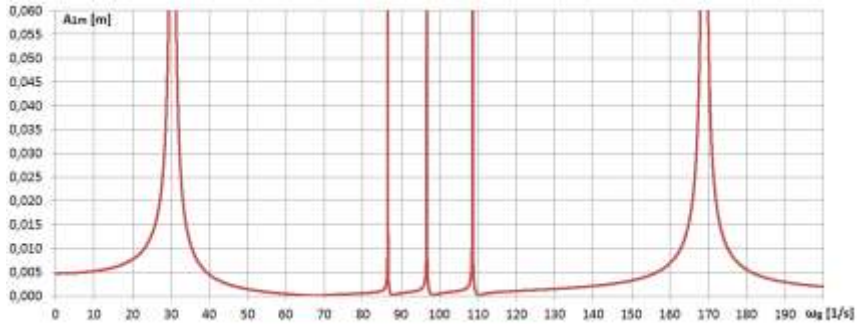

Figure 5

Amplitude – excitation frequency diagram for the 5-DoF cantilever-mass mechanism

According to the already published paper [18], the vibration amplitude A_{1t} of the mass m_1 in the 5-DoF 'wallpaper' model with translator motion (Fig. 1b) is

$$A_{1t} = \frac{F_0}{\sqrt{(s_1 - m_1\omega_g^2 - \sum_{i=2}^{5} m_i G_{i1}\omega_g^2 cos\varphi_i)^2 + (k_1\omega_g + \sum_{i=2}^{5} m_i G_{i1}\omega_g^2 sin\varphi_i)^2}} \tag{30}$$

where $G_{i1} = \sqrt{\frac{\left(2D_i\omega_g\omega_i^{-1}\right)^2 + 1}{\left(1-\omega_g^2\omega_i^{-2}\right)^2 + \left(2D_i\omega_g\omega_i^{-1}\right)^2}}$, $\varphi_i = arc\ tg \frac{\omega_g\omega_i^{-1}}{(2D_i)^{-1}\left(\omega_g\omega_i^{-1}\right)^{-2} - (2D_i)^{-1} + 2D_i}$,

$$D_i = \frac{k_i}{2m_i\omega_i}, \quad \omega_i = \sqrt{\frac{s_i}{m_i}} \tag{31}$$

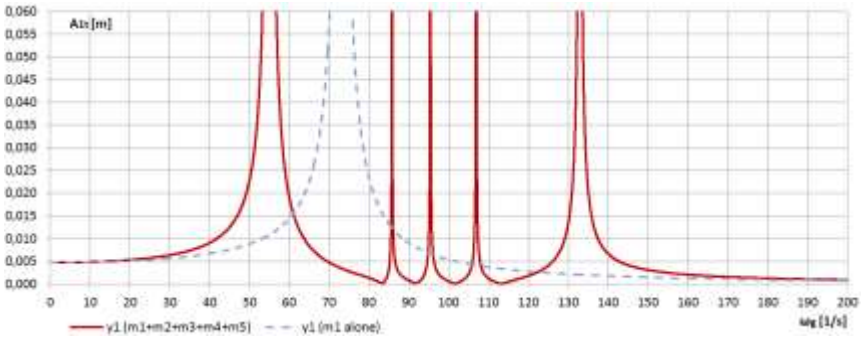

Figure 6

Amplitude - excitation frequency diagram for the 5-DoF translational model (solid line) and for 1-DoF translational model without absorber (dashed line)

In Fig. 6 the amplitude diagram as the function of the excitation frequency for the translator model (Fig. 1b) is plotted.

Comparing Fig. 5 and Fig. 6, it is visible that for both models (cantilever-mass and translational model, respectively) there are five resonances and four stopping positions (A_1=0) which are not at the same excitation frequencies. The three center resonances are almost at the same frequencies and the shape of the curves are similar. Positions of the first and the last resonances are different. The stopping frequencies of the cantilever model are smaller than of the other one.

In Fig. 7, the first six modal forms are presented for frequencies ω_1, ω_2, ... ω_6 of the 5-DoF cantilever-mass mechanism modelled as 3D solid body model (Fig. 2a). The FEA Mesh settings are: average element size is 0.100, minimum element size is 0.200, grading factor is 1.500, minimum turn angle is 60.00 deg, and curved mesh and elements are allowed. Local mesh control has to be in the interval 1.00 mm to the upper and lower side of the cantilever beam.

The results of the FEA can be seen as follows:

ω_1 – All the five masses vibrate in the same phase. This is the lowest resonance angular frequency of the main mass m_1.

ω_2 – Mass m_1 stops, the mass m_5 attached with the longest stick resonates. This is the lowest angular frequency of vibration suppression.

ω_3 – Mass m_1 stops, the mass m_4 attached with the second longest stick resonates. This is the second lowest angular frequency of vibration suppression.

ω_4 – Mass m_1 stops, attached mass m_3 and mass m_2 resonate together. This is the third lowest angular frequency of vibration suppression. It is interesting that there are no two different resonance frequencies in the FEA where mass m_3 and mass m_2 resonate separately as it is expected.

ω_5 – System makes torsion movements. This is irrelevant for the present investigation.

ω_6 – The main mass and the attached masses vibrate in the opposite phase. This is the highest resonance angular frequency from the two models' point of view.

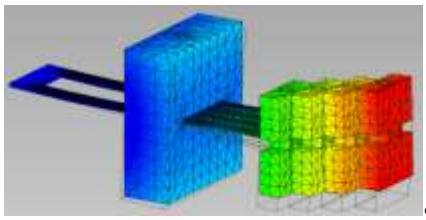
a)
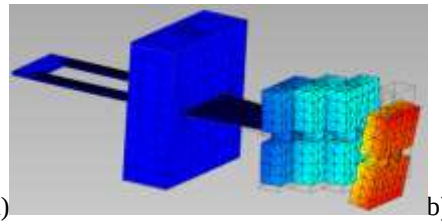
b)

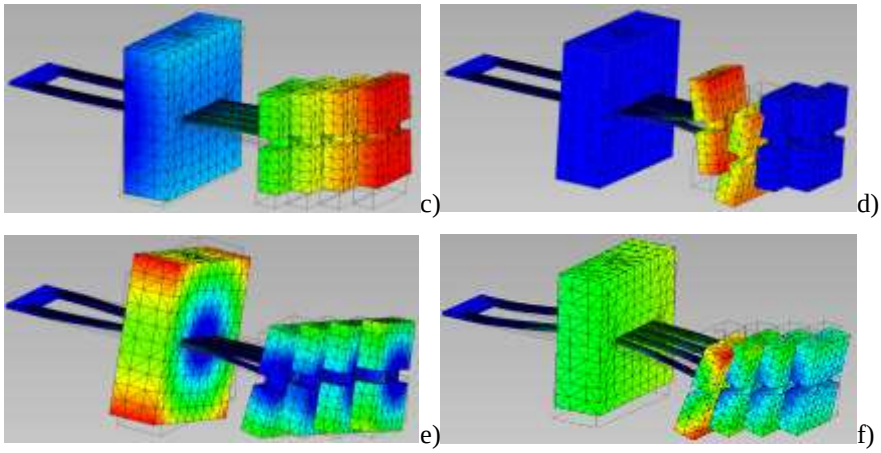

Figure 7
First six modal forms of FEA obtained by AutoDESK Inventor for frequencies: a) ω_1, b) ω_2, c) ω_3, d) ω_4, e) ω_5, f) ω_6

The angular frequencies ω_2, ω_3, ω_4 of Inventor FEA fit well with the first three stopping (A_1=0) angular frequencies of the translational model, while the first and sixth ones support the values for the cantilever-mass model (Table 1).

Table 1
Frequencies of vibration for translational and cantilever

	Translational model ω [rad/s]	Cantilever model ω [rad/s]	Inventor Finite Element Analysis for cantilever model ω [rad/s]		
A_1= 0 m	**83,21**	67,26	ω_2 →	**83,38**	m_5 moves
	91,65	**87,73**	ω_3 →	**92,05**	m_4 moves
	101,60	**98,24**	ω_4 →	**102,16**	m_2 and m_3 moves in opponent phase
	113,05	**110,28**	no matches		
			ω_5 →	135,40	Torsion
A_1 in resonance	55,06	**30,42**	ω_1 →	**29,34**	m_1 and the attached masses vibrates in phase
	85,76	**86,53**	no matches		
	95,39	**96,68**			
	106,88	**108,58**			
	132,87	**168,94**	ω_6 →	**159,72**	m_1 and the attached masses vibrates in opposite phase

According to the calculations, it is seen that in both models, the four attached masses stop the main mass at four different frequencies. However, some inconvenient resonances exist. Their decrease is obtained by using the dampers.

In Fig. 8, the amplitude-frequency diagram for various values of the damping in the translational model is considered. It shows the calculations of the translational model with relatively small damping values set for all (k_i=*0-5 Ns/m*), while the lowest critical damping value is much higher (k_{5crit}=*2 m*ω_5=*83,21 Ns/m*).

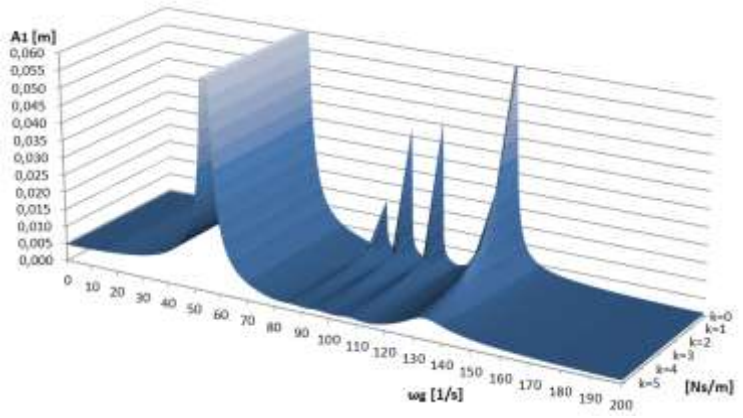

Figure 8
Amplitude-frequency-damping curve for m_1 at translational model

In Fig. 8, it is found that in the translational model (even for small damping) the amplitudes of vibration have the tendency of decrease in the excitation frequency range of 65 – 120 rad/s. Based on this result, it is expected that the same property is evident in cantilever-mass model.

Conclusions

In the paper, the multicantilever-mass mechanism for vibration suppression is considered. The physical model contains the system of clamped beams with attached masses which act as vibration absorbers. The mathematical model of the system is available for calculation of the amplitude of vibration for different excitation frequencies. Based on 1-DoF measurements, an elastic supporting theory was introduced for the calculating of the torque spring stiffness of clamping of the beam end. It is shown that the measured and calculated stiffness are in good agreement. In addition, it is concluded in the paper that a comparison between the cantilever mechanism suggested in the paper and the already existing translational model is possible. For certain frequency values, i.e. for the second, third and fourth frequencies, vibration is suppressed in both models. In addition, the amplitude-frequency plots for both models are similar in shape. Both models are in good agreement with numerical results matched with the Inventor FEA, too. However, it is obvious that the difference in results for the cantilever-mass system and translation mechanism is negligible.

Due to its simplicity (in comparison to the metastructure with translational motion of masses), the chosen cantilever system would be appropriate for measurements and future experimental investigation. The obtained experimental results for cantilever-mass mechanism should be treated for metastructure analysis.

As a final result of the investigation, the influence of damping in the 5-DoF metastructure was measured and calculated. It was highlighted that as the damping increases, the amplitudes of vibration for three medium resonance frequencies decrease dramatically.

For further investigation, the physical and mathematical model of the 'wallpaper' type metastructure's basic cell (with one coupled mass) can be developed.

Acknowledgement

This research did not receive any specific grant from funding agencies in the public, commercial, or not-for-profit sectors.

References

[1] Y. Cheng, J. Y. Xu, X. J. Liu, One-dimensional structured ultrasonic metamaterials with simultaneously negative dynamic density and modulus, Physical Review B, 2008, 77(4) 045134

[2] R. Zhu, X. N. Liu, G. K. Hu, C. T. Sun, G. L. Huang, A chiral elastic metamaterial beam for broadband vibration suppression, Journal of Sound and Vibration 333(10), 2014, pp. 2759-2773

[3] K. K Reichl, D. J. Inman Lumped mass model of a 1D metastructure for vibration suppression with an additional mass, Journal of Sound and Vibration 403, 2017, pp.75-89

[4] K. K. Reichl, D. J. Inman, Lumped mass model of a 1D metastructure with vibration absorbers with varying mass, in Sensors and Instrumentation, Aircraft/Aerospace and Energy Harvesting (eds. E.W. Sit), Vol. 8, Conf. Proceedings of the Society for Experimental Mechanics Series, 2019, pp. 49-56

[5] Y. R. Wang, T. Wen Liang, Application of lumped-mass vibration absorber on the vibration reduction of a nonlinear beam-spring-mass system with internal resonances, Journal of Sound and Vibration, 350,2015, pp. 140-170

[6] H. Sun, X. Du, P. F. Pai: Theory of metamaterial beams for broadband vibration absorption, Journal of Intelligent Material Systems and Structures, 21, July, 2010, pp. 1085-1101

[7] P. F. Pai, H. Peng, S. Jiang: Acoustic metamaterial beams based on multifrequency vibration absorbers, International Journal of Mechanical Sciences, 79, 2014, pp. 195-205

[8] P. F. Pai, Metamaterial-based broadband elastic wave undamped vibration absorber. Journal of Intelligent Material Systems and Structures 21(5), 2010, pp. 517-528

[9] L. Cveticanin, Gy. Mester, Theory of acoustic metamaterials and metamaterial beams: An overview, Acta Polytechnica Hungarica, 13(7), 2016, pp. 43-62

[10] Milton GW. (2007) New metamaterials with macroscopic behavior outside that of continuum elastodynamics. New Journal of Physics 9, 2007, 359:pp. 1-13

[11] H. Sun, X. Du, R. R. Pai, Theory of metamaterial beams for broadband vibration absorption, Journal of Intelligent Material Systems and Structures, 21 July 2010, pp. 1085-1101

[12] P. F. Pai, H. Peng, S. Jiang, Acoustic metamaterial beams based on multi-frequency vibration absorbers, International Journal of Mechanical Sciences, 79, 2014, pp. 195-205

[13] T. Wang, M. P. Sheng, Q. H. Qin, Multi-flexural band gaps in an Euler-Bernoulli beam with lateral local resonators, Physics Letters A, 380, 2016, pp. 525-529

[14] M. Askari et al.: Additive manufacturing of metamaterials: A review, Additive Manufacturing 36, 2020, 101562

[15] X. Yu et al., Mechanical metamaterials associated with stiffness, rigidity and compressibility: A brief review, Progress in Material Science 94, 2018, pp. 114-173

[16] H. Peng, P. F. Pai, Acoustic metamaterial plates for elastic wave absorption and structural vibration suppression, International Journal of Mechanical Sciences, 89, 2014, pp. 350-361

[17] H. Peng, P. F. Pai, H. Deng, Acoustic multi-stopband metamaterial plates design for broadband elastic wave absorption and vibration suppression, International Journal of Mechanical Sciences, 103, 2015, pp. 104-114

[18] P. Szuchy, 5-Degree-of-freedom systems in acoustic metamaterials, International Scientific Conference ETIKUM 2018,Proceedings, 6-8 December 2018, ISBN 978-86-6022-123-2 Novi Sad, Serbia, 2018

[19] J. D. Hobeck, C. M. V. Laurent, D. J. Inman, 3D printing of metastructures for passive broadband vibration suppression, 20th Int. Conf. on Composite Materials, Copenhagen, 19-24 July, 2015, pp. 1-8

[20] C. D. Pierce, C. L. Willey, V. W. Chen, J. O. Hardin, J. D. Berrigan, A. T. Juhl, K. H. Matlack, Adaptive elastic metastructures from magneto-active elastomers, Smart Material Structure 29, 2020, 065004, pp. 1-11

[21] B. C. Essink, D. J. Inman, Three-dimensional mechanical metamaterial for vibration suppression, Special Topics in Structural Dynamics & Experimental Techniques (Ed. N. Dervilia), Vol. 5, 2020, pp. 43-48

[22] L. Fan, Y. He, X. Chen, X. Zhao, Elastic metamaterial shaft witth a stack – like resonator for low-frequency vibration isolation, Journal of Physics D, Applied Physics, 53, 2020, 105101, pp. 1-9

[23] L. Cveticanin, M. Zukovic, Negative effective mass in acoustic metamaterial with nonlinear mass-in-mass subsystems, Communications in Nonlinear Science and Numerical Simulation, 51, 2017, pp. 89-104.

[24] L. Cveticanin, M. Zukovic, D. Cveticanin, On the elastic metamaterial with negative effective mass, Journal of Sound and Vibration, 2018, 436, pp. 295-309

[25] L. Cveticanin, M. Zukovic, D. Cveticanin, Influence of nonlinear subunits on the resonance frequency band gaps of acoustic metamaterial, Nonlinear Dynamics, 93(3), 2018, 1341-1354

[26] T. Wang, M. P. Sheng, Q. H. Qin, Multi-flexural band gaps in an Euler-Bernoulli beam with lateral local resonators, Physics Letters A, 2016, 380, pp. 525-529